Cyclometalated luminescent platinum(II) complexes of dissymmetrical 2,2':4',2"–terpyridine and its self–assembled dimer presenting Pt–Ag dative bonds

Lorien Benda, Louise Miton, Hadj Seyd, Lise–Marie Chamoreau, Gediminas Jonusauskas, Nathan D Mcclenaghan, Bernold Hasenknopf, Valérie Marvaud, Guillaume Vives

Cyclometalated luminescent platinum(II) complexes of dissymmetrical 2,2':4',2"-terpyridine and its self-assembled dimer presenting Pt-Ag dative bonds

Lorien Benda,[a‡] Louise Miton,[a‡] Nihal Hadj Seyd,[a] Lise-Marie Chamoreau,[a] Gediminas Jonusauskas,[c] Nathan D. McClenaghan,[b] Bernold Hasenknopf,[a] Valérie Marvaud,[a] and Guillaume Vives*[a]

A series of cyclometalated (N^C^N) Pt(II)-platinum complexes featuring a terpyridine ligand with a non-coordinating nitrogen atom and a Pt-C bond was synthesized. In the presence of Ag^+, the bis(isonitrile)Pt(II) complex formed a remarkable self-assembled helicoidal dimer stabilized by coordination of Ag(I) and metallophilic Pt-Ag interactions. Its assembly was observed in the solid state and maintained in solution. All complexes show strong luminescence and multiple emitting states, which could be rationalized based on solid state X-ray structures and coordinating environment.

Introduction

Since its first synthesis by Morgan and Burstall,[1] terpyridine and its derivatives[2] have been widely used as versatile ligands to form a variety of complexes for applications in coordination, supramolecular, biological or materials chemistry.[3] In particular, terpyridine platinum(II) complexes and their cyclometalated analogues have attracted wide interest for their luminescence and role in self-assembly.[4] Compared to (N^N^N) ligands, cyclometalated (N^C^N) or (C^N^N) Pt(II) complexes present enhanced luminescence due to the strong sigma-donating ability of such ligands that increase the energy gap between ^{3}MC and ^{3}LC states thereby reducing non radiative deexcitation and promoting higher photoluminescence quantum yields.[5] In addition, the square planar geometry of Pt(II) complexes is well-suited for establishing Metal-Metal interactions between closed or pseudo-closed-shell metal ions.[6] Due to their strong ligand field, cyclometalated ligands induce the formation of stronger Pt-M dative bonds thanks to the high energy of the dz^2 platinum orbital. Such Pt-M dative bonds can exhibit interesting luminescence properties.[7]

During the course of our work on switchable molecular tweezers based on terpyridine(M-salen)$_2$ complexes,[8] an unexpected 2,2':4',2"-terpyridine was readily obtained instead of the usual symmetrical 2,2':6',2" isomer using Kröhnke synthesis conditions (Figure 1). Typically such dissymmetrical terpyridine isomers have been largely unexplored as ligands due to their low accessibility.[9] In fact, they are obtained as a minor product of the terpyridine condensation reaction and require tedious purifications, usually involving separation from the symmetrical terpy by precipitation of its Fe(II) complex as originally developed by Sauvage.[9b] Nevertheless, dissymmetrical terpyridine regioisomers appeared to be well suited to obtain cyclometalated (N^C^N) terpyridine-platinum(II) complexes analogous to the well-known (N^C^N) complexes with dipyridylbenzene ligand. Our aim was to evaluate the effect of the nitrogen heteroatom on the central cyclometalated ring on the photophysical and self-assembly properties of the Pt(II) complexes.

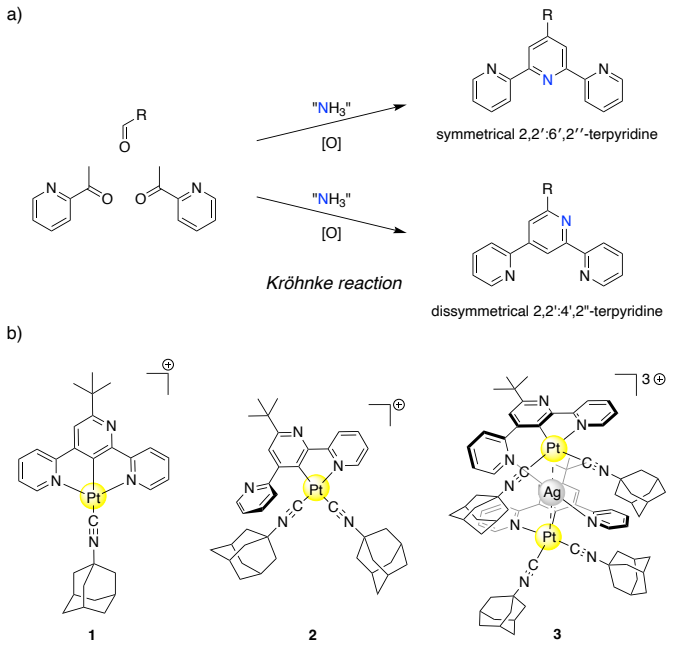

Figure 1. a) Possible terpyridine isomers obtained from one-pot Kröhnke condensation between acetylpyridine and an aldehyde. b) Herein reported cyclometalated (N^C^N) platinum complexes with a dissymmetrical terpyridine ligand.

Herein we report an efficient synthesis of a new dissymmetrical 2,2′:4′,2′′-terpyridine ligand and its Pt(II)-cyclometalated complexes with one or two isonitrile ligands (noted **1** and **2** respectively) (Figure 1). Complex **2** presents a free pyridine moiety that was used to bind to Ag(I) and obtain the self-assembled dimer **3** presenting metallophilic Pt-Ag-Pt interactions. The photophysical properties of these luminescent complexes are also reported.

Results and discussion

Ligand synthesis

Terpyridine ligands are usually obtained by a condensation reaction to form the central pyridine ring under conditions described by Hantzsch, Tschitschibabin, Jameson, Kröhnke or Potts.[2b] The synthesis of symmetrical 4′-tert-butyl-2,2′:6′,2′′-terpyridine **4a** has been described by Constable[10] by the treatment of 2-acetylpyridine by ^{t}BuOK with pivalaldehyde in THF followed by cyclization with NH_4OAc in glacial acetic acid. However, when we performed the reaction with KOH and NH_4OH in methanol, the 2,2':4',2"-terpyridine isomer **4b** was surprisingly obtained in 46% yield with only traces of the 2,2′:6′,2′′-terpyridine regioisomer. Terpyridine **4b** was easily purified by column chromatography and was unambiguously characterized by 2D NMR spectroscopy and mass spectrometry.

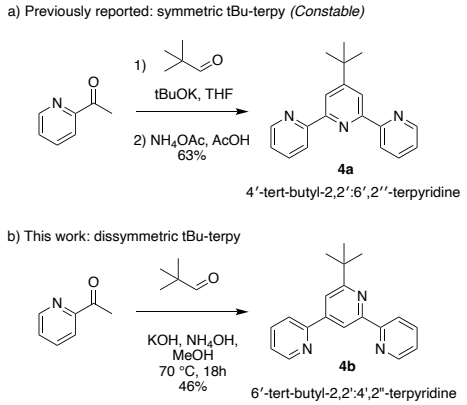

Scheme 1. a) Reported synthesis of 4′-tert-butyl-2,2′:6′,2′′-terpyridine **4a** by Constable. b) Synthesis of the dissymmetrical regioisomer 6′-tert-butyl-2,2′:4′,2′′-terpyridine **4b**.

The formation of such a regioisomer can be explained by examining its reaction mechanism[11] (see Scheme S1). First, the deprotonation of acetylpyridine yields an enolate that performs a nucleophilic attack on the electrophilic carbon of the pivalaldehyde. After crotonylation, an α-enone intermediate is formed and can undergo a nucleophilic addition by a second acetylpyridine enolate with either 1,4- or 1,2-regioselectivity. The symmetrical terpyridine is obtained by a 1,4-nucleophilic addition while the 1,2-addition yields terpyridine regioisomer **4b**. The regioselectivity in the addition appears to be controlled by the solvent, with polar protic methanol favoring the 1,2-addition under charge control while THF preferentially yielded the 1,4-addition product under orbital control. The steric hinderance of the tert-butyl group seems to play an important role disfavoring the 1,4-addition in our case as the 1,2-addition product is rarely obtained as major product with benzaldehyde derivatives.[9b] Indeed, 2,2':4',2"-phenylterpyridine analogs are only obtained as a minor product and present considerable challenges in separation from the major symmetrical 2,2′:6′,2′′-terpyridine isomer. Thus, the inversion in regioselectivity observed with pivaldehyde enables the facile access to this unusual terpyridine regioisomer and allows exploring its ligating properties.

Synthesis and characterization of monometallic Pt-complexes

This new terpyridine ligand **4b** was evaluated in the synthesis of cyclometalated (N^C^N) platinum complexes in order to assess the effect of the heterocyclic central ring on the photophysical properties compared to phenyl analogues.[12] A typical strategy for cyclometalated platinum complexes was employed through the versatile intermediate [Pt-(N^C^N)Cl] complex **5.** By heating **4b** in presence of K_2PtCl_4 at 120°C in acetic acid for 3 days, complex **5** was obtained in 75% yield as a yellow solid (Scheme 2). Single crystals were obtained by slow evaporation of an acetonitrile solution of **5** (Figure 2). The complex crystallizes in the monoclinic space group $P2_1/m$, with a 1028 Å^3 cell size (a = 12.6144 Å; b = 6.7077 Å; c = 12.6960 Å; α = γ = 90°; β = 106.73°). The tetracoordinated Pt(II) is located in the plane formed by the N^C^N ligand and the chlorine atom. It adopts a slightly distorted square plane geometry with N-Pt, C-Pt, N-Pt, and Pt-Cl distances of 2.039, 2.018, 2.040, 2.399 Å, respectively. The presence of the tert-butyl group favors a head-to-tail arrangement between two Pt complexes with an interplanar distance of 3.354 Å as expected for π-stacking. In contrast, the Pt-Pt distance of 5.139 Å is too large to observe any Pt-Pt interactions in the crystalline state.

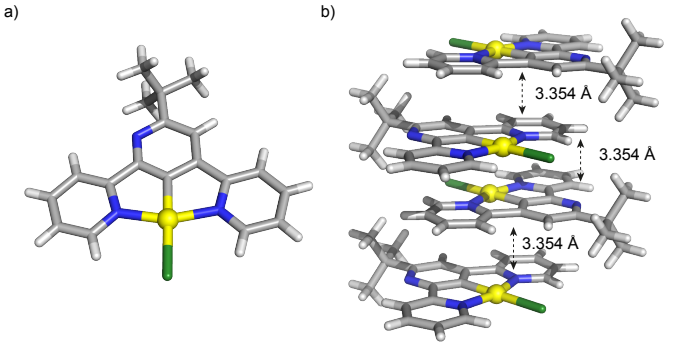

Figure 2. Crystallographic structure of a) complex [Pt(**4b**)Cl] (**5**) and b) its head to tail columnar packing with π-stacking interactions.

Then, we investigated the exchange of the labile chloride ligand of complex **5** with isocyanoadamantane to achieve cationic luminescent cyclometalated complexes. An adamantyl moiety was selected due to the higher stability of the isonitrile and the high affinity of adamantyl for cyclodextrin and cucurbituril macrocycles, which would allow the formation of host-guest complexes in aqueous media.[13] Complex [Pt(**4b**)Cl] (**5**) was first reacted with AgOTf in CH_2Cl_2, followed by addition of isocyanoadamantane. This synthesis, performed with 1.1 equiv. of AgOTf and isonitrile ligand, led to the formation of complex [Pt(**4b**)(CN-Ad)]OTf (**1**) in 51% yield. Complex **1** was fully characterized by NMR and mass spectrometry. The same procedure with 2.0 equiv. of isocyanoadamantane

ligand resulted in complex [Pt(**4b**)(CN-Ad)$_2$]OTf (**2**) where two isonitrile ligands are coordinated to the platinum thus displacing one pyridine of the terpyridine ligand. This is clearly visible in the ^{1}H NMR spectrum with the presence of two non-equivalent isocyanoadamantane ligands presenting the same diffusion coefficient as the rest of the molecule according to DOSY NMR (Figure S1). The TROESY spectrum (see Figure S2) provided further insight on the geometry of complex **2** with exclusive cross-correlations between H_{11a} protons of one adamantyl ligand and H_6 pyridine protons while the H_{11b} protons of the second adamantyl presents correlations with protons of the other side pyridine H_5, H_4 and H_3. This indicates a selective decoordination of the pyridine ring opposite to the central nitrogen that enables its free rotation and NOE correlation with the isonitrileadamantyl ligand in close proximity. Such unusual decoordination of a chelating terpyridine ligand has only been previously observed with very strong sigma donor ligands such as NHC or isonitriles.[14] This free pyridine moiety was further exploited in the present study as coordination site in a self-assembled metallosupramolecular structure.

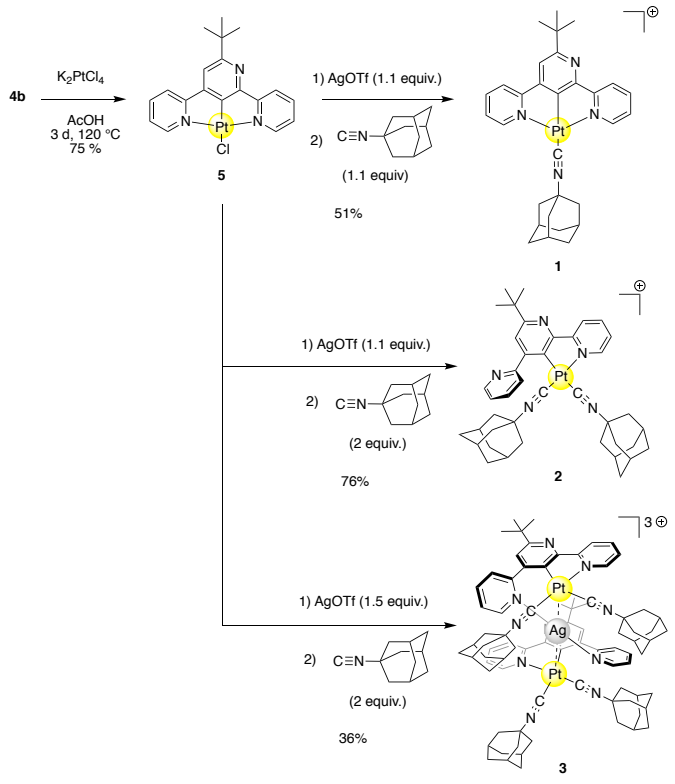

Scheme 2. Synthesis of cyclometalated Pt-(N^C^N) complexes.

Self-assembled trinuclear dimer

Complex **2**, prepared *in situ* from **5** and isocyanoadamantane but with an excess of Ag(OTf) (1.5 equiv.), resulted in a drastically different product (**3**). The ^{1}H NMR spectrum, compared to complex **2**, features a strong upfield shift for terpy protons H_6 and H_1 and downfield shift for H_5 (see Figure S3). In addition, the diffusion coefficient of this new species in CD_2Cl_2 ($1.60 \cdot 10^{-9}$ $m^2.s^{-1}$) is significantly lower than the related complex **2** ($2.23 \cdot 10^{-9}$ $m^2.s^{-1}$) indicating a significant increase in size compared to the latter. Single crystals of compound **3** could be obtained by slow evaporation of the solution in $CHCl_3$ revealing that **3** is a dimer assembled by a bridging Ag(I) coordinated to the free pyridine moiety of two molecules of **2**. The dimer crystallizes in the $P2_1/n$ space group, with a 9864 Å^3 cell size (a = 15.445 Å; b = 42.457 Å; c = 15.612 Å; α = γ = 90°; β = 105.52°). The self-assembled dimer adopts a helicoidal structure stabilized by additional Pt-Ag-Pt dative bonds. A mixture of *M* and *P* helicity is observed in the centrosymmetric packing indicating no spontaneous resolution. The coordination spheres of both Pt(II) ions, of pseudo-square planar geometry, consist of Pt-$C_{isonitrile}$ bonds of 1.853 and 1.846 Å as well as a Pt-N and Pt-C bond to the terpyridine ligand of 2.048 and 1.950 Å respectively. Ag(I) is coordinated to two nitrogen atoms from one of the pyridines of each of the two terpyridine ligands in a quasi-linear geometry with an N-Ag-N angle of 176.22° and N-Ag distances of 2.179 and 2.216 Å usual for Ag-pyridine complexes. More interestingly, Ag is in close contact with the two Pt(II) atoms forming two metal-metal interactions with Pt-Ag distances of 2.850 and 2.868 Å. These distances are comparable with Pt-Ag dative bond reported in the literature[15] with cyclometalated Pt(II) complexes (2.67-2.94 Å). The three atoms are slightly bent with a Pt-Ag-Pt angle of 159.0°. The cyclometalated terpyridine and strong σ-donating isonitrile ligands of complex **2** are well suited to stabilize such dative bonds as they raise the energy of the platinum dz^2 orbitals allowing for stronger metallophilic interactions with Ag(I). It should be noted that the dimeric structure of **3** is similar to the one described in the literature for a platinum(II) complex coordinated with a chiral cyclometalated (N^C^N) dipyridylbenzene ligand and two 2,6-dimethylphenyl isonitrile ligands.[14a] However, the authors surprisingly report a bridging Pt(II) ion instead of Ag(I) here. Their attribution appears questionable due to what would be a very unusual geometry for a Pt(II) and the presence of $AgClO_4$ during their synthesis.

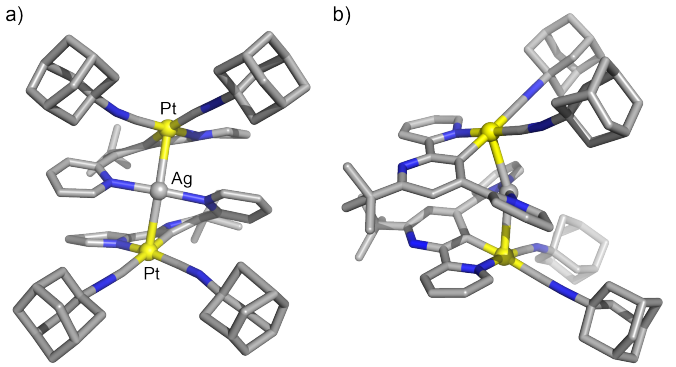

Figure 3. Crystallographic structure of self-assembled Pt(II) dimer **3** a) front and b) side view (solvent, counter anions and hydrogens have been omitted for clarity).

In order to assess the stability of dimer **3** in solution, 2D NMR experiments were carried out in $CDCl_3$. NOE

correlations between adamantyl protons H_{11a} and protons H_5, H_4 and H_6 belonging to two opposite pyridine rings on the terpy are in agreement with the dimeric structure observed in the solid state (Figure 4). Indeed, the distances of 3.063 and 2.396 Å between H_{11a} and the H_5 and H_4 protons of the second Pt complex are compatible with NOE correlation. On the other hand, the adamantyl proton H_{11b} presents cross-correlation with protons H_3, H_4 and H_5 belonging to the pendant pyridine moiety. This observation is also in agreement with the helicoidal dimeric structure as the second adamantyl is in close proximity to only such a pyridine. The strong upfield shift of H_1 proton is also explained by its position in the shielding cone of the second pyridine moiety. The presence of a dimeric structure in solution was also confirmed by mass spectrometry with a signal at *m/z* = 1903.52 and 2017.50 (see Figure S4) corresponding to dimers $[\mathbf{3}(OTf)(Cl)]^+$ and $[\mathbf{3}(OTf)_2]^+$, respectively. All of these observations indicate the helicoidal dimeric structure observed in the solid state is also present in solution. Such a remarkable self-assembled structure is obtained by a combination of Ag-N coordination bond to the free pyridine moiety and Ag-Pt dative bonds.

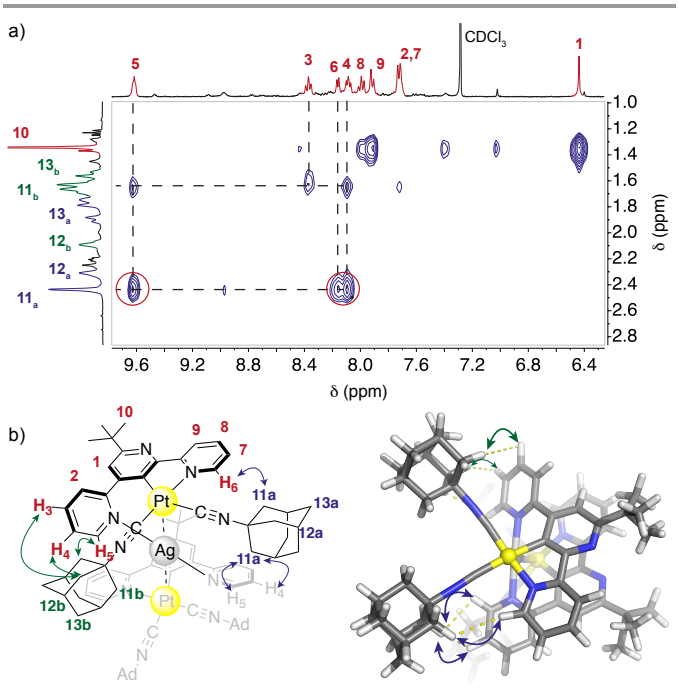

Figure 4. a) ^{1}H NMR NOESY Spectra (600 MHz, $CDCl_3$, 300K) of dimer **3** showing correlation between adamantyl protons H_{11a} and pyridine protons H_6 and $H_{4\text{-}5}$ of both Pt(II) moieties. b) representation of selected correlation in the crystallographic structure.

Spectroscopic properties

The spectroscopic properties of the complexes were evaluated by electronic absorption and emission spectroscopies in dilute solution (Figure 5). All three complexes (**1** – **3**) exhibit qualitatively similar absorption spectral profiles in $CHCl_3$. The intense bands in the region 280 – 320 nm with large molar absorption coefficients (~10^4 mol^{-1} l cm^{-1}) are attributed to ^{3}IL π–π* transitions localized on the cyclometalated terpyridine ligand, and are essentially doubled for dimer **3** *c.f.* **1** & **2**. The lower energy near-UV bands are attributed to mixed charge-transfer/intraligand transitions within the complexes by analogy with reported cyclometalated complexes.[16]

The steady-state emission spectra of complexes **1** and **2** are dominated by a band (λ_{max} = 497 and 498 nm, respectively) with a vibronic progression characteristic of terpyPt complexes.[12a, 12d] The emission maxima are similar to reported Pt complex with dipyridylbenzene ligand with isonitrile ligands.[12a, 14a, 17] The emission from dimer **3** appears slightly red-shifted with less pronounced vibronic structuring. In terms of quantum yields in rigorously degassed solution, the mononsubstituted complex **1** proved significantly more luminescent (Φ_{lum} = 0.21) than reported N^C^N analogs (Φ_{lum} = 0.12-0.14) demonstrating the effect of an heteroatom on the central ring. However, the bis(isonitrile) complex **2** displayed a lower emission (Φ_{lum} = 0.05) probably due to the loss of rigidity induced by the free pyridine moiety. Upon coordination of this pyridine moiety to Ag(I) in the dimer **3**, some luminescence was recovered (Φ_{lum} = 0.12). Among the cyclometalated complexes tested, intermediate complex **5** was the most emissive at room temperature (Φ_{lum} = 0.35) yet remained significantly lower than the recently reported record value (0.81) for a N^C^N Pt(II) complex with 1,3-di(pyrimidin-2-yl)benzene ligand.[18]

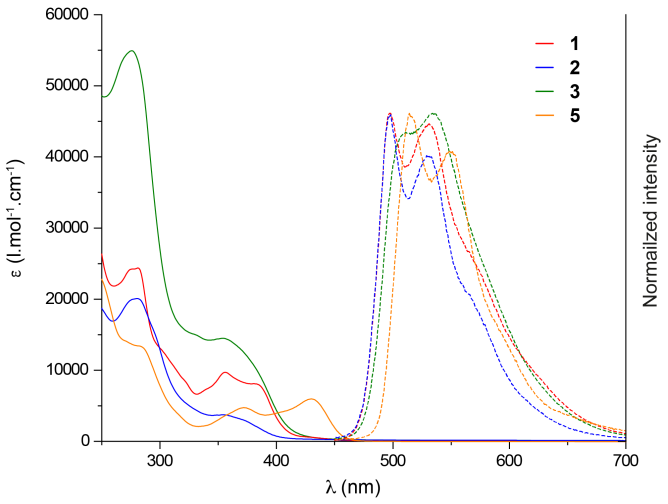

Figure 5. Absorption and normalized emission spectra (dashed) of complexes **1**, **2** and **3**, (5 10^{-5} mol.l^{-1} in $CHCl_3$, 298 K, λ_{ex}= 400 nm).

Table 1. Photophysical data for complexes **1**-**3**, **5** in degassed $CHCl_3$ solution.

	λ_{abs}[nm] (ε [L·mol^{-1}cm^{-1}])	λ_{em} [nm]	τ_{em} [μs]	Φ_{em}	k_r /10^3 [s^{-1}]	$\sum k_{nr}$ /10^3 [s^{-1}]
1	278 (24 000) 356 (9 700) 384 (8 000)	497 531	8.8	0.21	24	90
2	279 (20 000) 357 (3 700)	498 531	5.8 (0.9) 10.1 (0.1)	0.05	8.6	160
3	275 (55 000) 355 (14 500)	510 534	7.4 (0.85) 19.4 (0.15)	0.12	16	120
5	284 (13 000) 373 (4 700) 430 (5 900)	514	11.4	0.35	31	57

Radiative, k_r, and nonradiative, $\sum k_{nr}$, rate constants estimated assuming that the emitting state is formed with unit efficiency such that $k_r = \Phi_{em}/\tau$ and $\sum k_{nr} = (1 - \Phi_{em})/\tau$.

To gain further insight into the excited-state properties of the luminescent complexes, time-resolved emission studies were undertaken on different timescales both at room temperature and in a frozen matrix at 77K (λ_{exc} = 355 nm in all cases). Figure 6 shows emission for representative molecule **2** at room temperature (Figure 6a) and at 77K (Figure 6b), see ESI for other emission spectra. In **1** - **3,** a very weak and prompt featureless nanosecond emission was noted in the 400-450 nm region, while the dominant more red-shifted emission decayed on the microsecond timescale at room temperature (τ = 8.8 μs for **1**; 5.8 μs (0.9) & 10.1 μs (0.1) for **2**; 7.4 μs (0.85) & 19.4 μs (0.15) for **3** and 11.4 μs for **5**). The emission lifetimes are significantly longer than dipyridylbenzene analogs Pt-complexes (3.5 – 5.5 μs).[11a] No grow-in of the major band suggests that the decay pathways are not interconnected. The origin of the rather small second decay component is tentatively ascribed to a small amount of association, and/or second sphere interactions. Considering radiative and non-radiative rate constants (Table 1), these appeared higher and lower, respectively, for molecules where all three terpy rings bound the same Pt ion (namely **1** and **5**), making these planar molecules the more emissive species. Structural distortion and a freely rotating uncoordinated pyridine ring may partly account for **2** being the least emissive species.

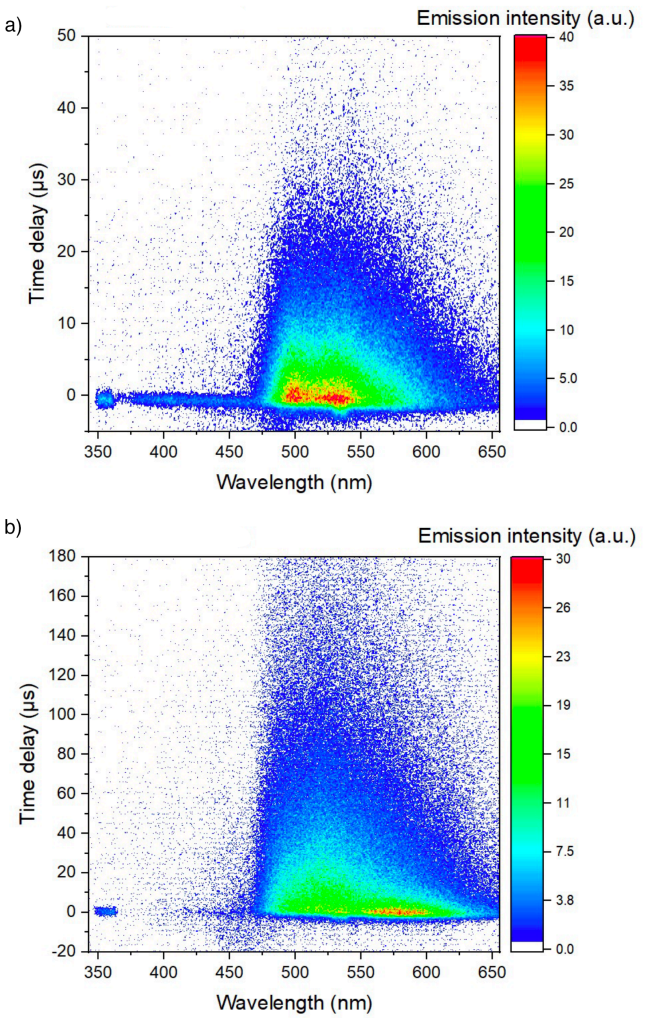

Figure 6. Emission of **2** in $CHCl_3$ (λ_{ex} = 355 nm). Emission recorded on streak camera at a) 100 μs scale at RT and b) 200 μs scale at 77 K.

Interestingly, low temperature emission in a frozen matrix (77K) featured an extra red-shifted band in the cases of **1**, **2**) and was most pronounced in the case of **5** (see Figure S13-16) which comprises the least sterically-congested coordination environment. This luminescence band decayed on a microsecond timescale (τ = 3.7 μs for **1;** 4.8 μs for **2;** 3.5 μs for **5**). This band was tentatively ascribed to an intermolecular Metal–Metal-to-Ligand Charge Transfer (MMLCT) emission involving close Pt-Pt approach. Such effects have been seen in a range of platinum complexes and metallo-gels.[19] This points to ground state aggregation even at micromolar concentration at low temperature (before freezing the matrix). However, this was notably absent in the case of dimer **3,** which may in part be due to the less planar adopted conformation which is less conducive to stacking.

Photoluminescence for **1**, **2**, **3** and **5** was further recorded in the solid state (Figure S17 - Sxxxx). While **1**, **2** and **3** showed qualitatively similar emission, progressive blue-shifting in the corresponding major emission band is noted (λ_{max} = 589 nm, 569 nm and 537 nm, respectively)

consistent with increasing structural rigidity or inhibition to excited-state structural relaxation. Correspondingly, emission decays increase from sub-microsecond for **1** to circa 5 μs for **3**. Furthermore, some vibronic fine structure starts to become visible in the emission spectrum of **3**, unlike the unstructured emission on **1** and **2**. In contrast, the solid-state emission of **5** lies much further towards the red (λ_{max} = 646 nm, τ = ca. 1 μs), suggesting emission emanates from a different excited-state in this case, anticipated to result from a dominant M-M interaction in the case of **5** in the non-crystalline solid state.

Conclusion

In conclusion, we report a facile synthesis of a dissymmetrical terpyridine ligand allowing the formation of cyclometalated (N^C^N) Pt(II) complexes with a nitrogen heteroatom on the central ring. The effect of such a heteroatom on the photophysical properties was investigated on complexes with isocyanoadamantane ligands. Compared to a central phenyl ring, the pyridine significantly increased the luminescence quantum yield while not shifting the emission maximum. In presence of an excess of isonitrile ligand, decoordination of one pyridine moiety was observed due to its strong σ-donating ability. This bis(isonitrile) complex formed a helicoidal self-assembled dimer around a bridging Ag(I). The dimer is stabilized by metallophilic Pt-Ag interactions and has been observed both in the solid state and in solution. This dimer's unique helicoidal structure revealed attractive emission properties, signaling a promising avenue for the development of innovative chiral luminescent materials. Such systems leveraging metallophilic interactions would offer potential applications in the realms of optoelectronics and sensor technology, among others.

Experimental section

General Analytical and Synthetic Methods. ^{1}H NMR and ^{13}C NMR spectra were recorded at 400 or 600 MHz on Bruker Avance III spectrometers. Chemical shifts (δ) are reported in ppm from tetramethylsilane using residual solvent peaks for calibration. Electrospray ionisation (ESI) mass spectrometry was performed on a Bruker microTOF spectrometer. Reagent grade tetrahydrofuran was distilled from sodium and benzophenone. All others chemicals were purchased from commercial suppliers and used without further purification. Flash column chromatography was performed using silica gel from Merck (40-63 μm) or GraceResolv High Resolution Flash Cartridges (particle size 40 μm). Thin layer chromatography was performed using aluminium plates pre-coated with silica gel 60 F254 0.20 mm layer thickness.

Photophysical studies. Solutions for spectroscopic studies were degassed (9×10^{-6} bar) by multiple freeze-pump-thaw cycles and the cell was blowtorch sealed. Electronic absorption spectra were recorded on dilute solutions in 1 cm quartz cells using a Varian Cary-50 spectrometer. Steady-state luminescence spectra were recorded on a Horiba Jobin-Yvon Fluorolog-3 spectrofluorometer equipped with a R928P PMT and were corrected. Quantum yields (Φ) of complexes were determined on comparison with an optically dilute $[Ru(bpy)_3]Cl_2$, bpy = 2,2'-bipyridine, standard (Φ_r) in air-equilibrated water (Φ_{em} = 0.042,[20] according to the equation: $\Phi = \Phi_r(I/I_r)(A_r/A)(\eta^2/\eta_r^2)$, where r is the reference, I is the integrated emission intensity, A is the absorbance at the excitation wavelength and η is the refractive index of the solvent. Luminescence lifetimes were measured on a on a set-up comprising a frequency tripled Nd:YAG amplified laser system with either nanosecond pulses (5 ns, 10 Hz, Ekspla model NT342B-10-WW) or picosecond pulses (30 ps, 20 Hz, Ekspla model PL2143A). Light signals were analysed by a spectrograph (Princeton Instruments Acton model SP2300) coupled with a high dynamic range streak camera (Hamamatsu C7700, sub-1 ns-1 ms). Accumulated sequences of pulses were recorded and treated by HPDTA (Hamamatsu) software to produce maps (wavelength vs delay) of transient emission intensity in the range 300 – 800 nm.

Compounds.

*Complex **1**: [Pt-(N^C^N)**4b**-(isocyanoadamantane)]OTf.*

In a round bottom flask, the complex [Pt-(N^C^N)-Cl] **5** (30 mg, 0.058 mmol, 1 eq) was dissolved in CH_2Cl_2 (10 mL). A solution of AgOTf (16 mg, 0.069 mmol, 1.1 eq) in MeOH (6 mL) was added. Then a solution of 1-isocyano-adamantane (10 mg, 0.069 mmol, 1.1 eq) in CH_2Cl_2 (2 mL) was added and the mixture was stirred overnight at room temperature. After evaporation of solvents, DCM was added and the resulting precipitate of AgCl was filtered off. The filtrate was evaporated, diethyl ether (6 mL) and hexane (6 mL) were added and the precipitate was then filtered over membrane yielding **1** as an orange solid (23 mg, 51%). ^{1}H NMR (600 MHz, 300 K, $CDCl_3$) δ 8.83 (d, J = 5.5 Hz, 1H), 8.62 (d, J = 5.8 Hz, 1H), 8.20 (td, J = 7.9, 1.4 Hz, 1H), 8.16 (td, J = 15.1, 7.7, 1.4 Hz, 1H), 8.12 (d, J = 7.7 Hz, 1H), 7.92 (d, J = 7.7 Hz, 1H), 7.74 (ddd, J = 7.7, 5.7, 1.4 Hz, 1H), 7.61 (ddd, J = 7.8, 5.6, 1.7 Hz, 1H), 7.36 (s, 1H), 2.38 (d, J = 2.3 Hz, 6H), 2.28 (s broad, 3H), 1.83 (d, J = 11.9 Hz, 6H), 1.77 (d, J = 12.8 Hz, 6H) 1.45 (s, 9H). ^{13}C NMR (151MHz, 300 K, DMSO-d_6) δ 167.7, 165.4, 164.3, 159.1, 158.1, 155.7, 155.5, 150.5, 142.1, 141.9, 127.7, 127.5, 123.4, 121.7, 119.6, 114.9, 58.7, 41.5, 38.0, 34.6, 30.2, 28.2. ESI-HRMS *m/z*: $[M\text{-}OTf]^+$ calc ($C_{30}H_{33}N_4Pt$) : 644.2353, found : 644.2351.

*Complex **2**: [Pt-(N^C^N)**4b**-(isocyanoadamantane)$_2$]OTf.*

In a round bottom flask, the complex [Pt-(N^C^N)-Cl] **5** (30 mg, 0.058 mmol, 1 eq) was dissolved in CH_2Cl_2 (10 mL). A solution of AgOTf (15 mg, 0.058 mmol, 1 eq) in MeOH (6 mL) was added. Then a solution of 1-isocyano-adamantane (19 mg, 0.116 mmol, 2 eq) in CH_2Cl_2 (2 mL) was added and the mixture was stirred overnight at room temperature.

After evaporation of solvents, DCM was added and the resulting precipitate of AgCl was filtered off. The filtrate was evaporated, diethyl ether (6 mL) and hexane (6 mL) were added and the precipitate was then filtered over membrane yielding **2** as an orange solid (42 mg, 76%). ^{1}H NMR (600 MHz, 300 K, CD_2Cl_2) δ 8.79 (d, *J* = 4.7 Hz, 1H), 8.72 (d, *J* = 5.7 Hz, 1H), 8.44 (d, *J* = 7.9 Hz, 1H), 8.20 (t, *J* = 7.6 Hz, 1H), 7.87 (t, *J* = 7.6 Hz, 1H), 7.75 (d, *J* = 7.6 Hz, 1H), 7.61 (t, *J* = 6.6 Hz, 1H), 7.47 – 7.45 (m, 2H), 2.24 (s, 9H), 2.08 (s broad, 3H), 1.77 (m, 6H), 1.73 (m, 9H), 1.65 (m, 3H), 1.46 (s, 9H). ^{13}C NMR (151 MHz, 300 K, CD_2Cl_2) δ 167.6, 164.2, 162.2, 152.2, 151.1, 150.0, 143.8, 142.2, 136.9, 126.6, 126.5, 123.9, 123.8, 122.5, 121.9, 120.3, 60.4, 60.2, 43.1, 43.0, 35.4, 35.3, 30.2, 29.3, 29.1. ESI-HRMS *m/z*: $[M\text{-}OTf]^+$ calc ($C_{41}H_{48}N_5Pt$): 805.3555, found: 805.3571.

*Dimer **3**: [(Pt-(N^C^N)**4b**-(isocyanoadamantane)$_2$)$_2$Ag](OTf)$_3$*
In a round bottom flask, the complex [Pt-(N^C^N)-Cl] **5** (50 mg, 0.096 mmol, 1 eq), was dissolved in CH_2Cl_2 (10 mL). A solution of AgOTf (37 mg, 0.145 mmol, 1.5 eq) in MeOH (6 mL) was added. Then a solution of 1-isocyano-adamantane (31 mg, 0.193 mmol, 2 eq) in CH_2Cl_2 (2 mL) was added and the mixture was stirred overnight at room temperature. After evaporation of solvents, DCM was added and the resulting precipitate of AgCl was filtered off. The filtrate was evaporated, diethyl ether (6 mL) and hexane (6 mL) were added and the precipitate was then filtered over membrane yielding **3** as an orange solid (76 mg, 36%). ^{1}H NMR (400 MHz, 300 K, $CDCl_3$) δ 9.59 (m, 2H), 8.35 (td, *J* = 7.7, 1.5 Hz, 2H), 8.14 (d, *J* = 5.7 Hz, 2H), 8.07 (m, 2H), 7.97 (td, *J* = 7.7, 1.0 Hz, 4H), 7.89 (dd, *J* = 7.7, 1.0 Hz, 2H), 7.71 – 7.69 (m, 4H), 6.41 (s, 2H), 2.41 (s, 12H), 2.29 - 2.22 (m, 6H), 2.07 (m, 6H), 1.81 (d, *J* = 12.8 Hz 6H), 1.70 (d, *J* = 12.8 Hz 6H), 1.60 – 1.56 (m, 24H), 1.32 (s, 18H). ^{13}C NMR (101 MHz, 300 K, $CDCl_3$) δ 167.5, 163.8, 162.5, 158.9, 154.6, 152.7, 152.4, 141.6, 141.2, 138.4, 128.1, 126.9, 124.8, 122.8, 122.7, 119.9, 119.6, 60.7, 60.2, 42.5, 42.1, 35.2, 35.1, 30.3, 29.0, 28.8, 28.7. ESI-MS *m/z*: $[M\text{-}(OTf)]^+$ calc ($C_{84}H_{96}AgF_6N_{10}O_6Pt_2S_2$): 2015.52, found: 2015.50.

*Ligand **4b**: 6'-tert-butyl-2,2':4',2"-terpyridine.*
In a sealed tube 2-acetylpyridine (1.0 g, 8.3 mmol, 2 eq) was dissolved in MeOH (50 mL). KOH (4.65 g, 83 mmol, 20 eq), trimethylacetaldehyde (0.355 g, 4.15 mmol, 1 eq) and NH_4OH (5.8 mL, 41.5 mmol, 10 eq) were added. The mixture was heated at 70°C during 18h. After evaporation of the solvent under reduced pressure, H_2O was added, and the aqueous layer was extracted with DCM. The organic layer was dried over $MgSO_4$ and evaporated. The crude product was purified by column chromatography (SiO_2: DCM/AcOEt, 100/0 – 70/30), yielding **4b** as a yellow viscous oil (568 mg, 46%). ^{1}H NMR (400 MHz, $CDCl_3$) δ 8.77 (s, 1H), 8.76 (d, *J*= 4.9 Hz, 1H), 8.70 (d, *J*= 4.9 Hz, 1H), 8.62 (d, *J*= 8.1 Hz, 1H), 8.10 (s, 1H), 8.02 (d, *J*= 7.8 Hz, 1H), 7.86 (td, *J*=1.4, 7.9 Hz, 1H), 7.81 (td, *J*= 1.4, 7.9 Hz, 1H), 7.34-7.31 (m, 2H), 1.51 (s, 9H). ^{13}C NMR (101 MHz, $CDCl_3$) δ169.7, 156.9, 156.0, 155.3, 150.1, 149.1, 147.9, 137.0, 136.9, 123.7, 123.6, 121.5, 121.5, 116.9, 115.4, 38.1, 30.5. ESI-HRMS *m/z*: $[M+Na]^+$ calc ($C_{19}H_{19}N_3Na$): 312.1471, found: 312.1461.

*Complex **5**: [Pt-(N^C^N)**4b**-Cl]*
In a Schlenk tube under argon, terpyridine **4b** (468 mg, 1.62 mmol, 1 eq) and K_2PtCl_4 (955 mg, 1.78 mmol, 1.1 eq) were dissolved in previous degassed acetic acid (70 mL). The mixture was heated at 120 °C during 5 days. After evaporation of the solvent under reduced pressure, few mL of MeCN were added, and the precipitate was filtered off and washed with methanol, ether and water. The solid was dissolved in DCM with a few drops of triethylamine yielding to the formation of a precipitate that was filtered off. The filtrate was evaporated under reduced pressure yielding **5** as a yellow solid (628 mg, 75%). ^{1}H NMR (400 MHz, 300 K, DMSO-d_6) δ 9.19 (d, *J* = 4.8 Hz, 1H), 9.12 (d, *J* = 5.0 Hz, 1H), 8.45 (d, *J* = 8.0 Hz, 1H), 8.38 – 8.26 (m, 4H), 8.09 (d, *J* = 7.3 Hz, 1H), 7.85 (s, 1H), 7.71 – 1.68 (m, 2H). ^{13}C NMR (101 MHz, 300 K, DMSO-d_6) 164.9, 164.4, 164.0, 156.8, 151.9, 151.7, 151.3, 147.9, 140.8, 140.5, 125.9, 125.7, 122.3, 120.6, 114.4, 39.7, 30.2. ESI-HRMS *m/z*: $[2M\text{-}Cl]^+$ calc ($C_{38}H_{36}N_6Pt_2Cl$): 1001.1965, found: 1001.1838.

Crystal structure determinations.
A single crystal of each compound was selected, mounted onto a cryoloop, and transferred in the cold nitrogen gas stream of an Oxford Cryostream. Intensity data were collected with BRUKER Kappa-APEXII diffractometers with either micro-focused Cu-Kα radiation (λ=1.54178 A) or sealed-tube Mo-Kα radiation at 200K. APEX 3 suite and SAINT program (BRUKER) were used to carry out data collections, unit-cell parameters refinements, integrations and data reductions. SADABS (BRUKER) was used for scaling and multi-scan absorption corrections. The structure were solved with SHELXT-14[21] program and refined by full-matrix least-squares methods using SHELXL-14.[22]

Details for **3**: crystals were grown by slow evaporation of a solution of **3** in $CHCl_3$. Light-orange crystals were obtained. Despite several tests, we had to carry out the data collection on a "not unique" and poorly diffracting sample, which lead to a low quality and low-resolution dataset. The low number of data prevented the anisotropic refinement of atoms other than platinum and silver ones. The presence of several chloroform molecules and of (disordered) triflate anions is one of the reasons for the low achievable resolution. Again, hydrogen atoms were placed at calculated positions and refined as a riding model. The position of the N atom on the central ring was determined from NMR NOESY correlation and from information about decoordination of one pyridine ring (complex **2**).
$C_{87.5}H_{97.5}AgCl_{7.5}F_9N_{10}O_9Pt_2S_3$, monoclinic, P21/n, a = 15.4562(9), b = 42.508(3), c = 15.6202(12), α = γ = 90°, β = 105.542(4)°, V = 9887.5(12) Å^3, Z = 4, radiation CuKα (λ = 1.54178), 36015 reflections measured, 8823 observed

[I ≥ 2σ(I)], 53 restraints 600 parameters, final R indices R_1 [I ≥ 2σ(I)] = 0.1270 and wR_2 (all data)= 0.3264, GOF = 1.052. CCDC number (2339432)

Details for **5**: yellow plate-like single crystals were obtained from a slow evaporation of a solution of 4b in acetonitrile. Data were treated as a twin (use of a HKLF5 file). Non-hydrogens atoms were refined anisotropically. Hydrogen atoms were placed at calculated positions and refined with a riding model.
$C_{21}H_{21}N_4ClPt$, monoclinic, P21/m, a = 12.6144(9), b = 6.7077(4), c = 12.6960(8), α = γ = 90°, β = 106.728(4)°, V = 1028.79(12) $Å^3$, Z = 2, radiation MoKα (λ = 0.71073), 29225 reflexion measured,
29225 observed [I ≥ 2σ(I)], 161 parameters, final R indices R_1 [I ≥ 2σ(I)] = 0.0558 and wR_2 (all data)= 0.1294, GOF = 1.111. CCDC number (2339433)

CCDC 2339432 – 2339433 contain the supplementary crystallographic data for this paper. The data can be obtained free of charge from The Cambridge Crystallographic Data Centre via www.ccdc.cam.ac.uk/structures.

Conflicts of interest

There are no conflicts to declare

Acknowledgements

Geoffrey Gontard (IPCM, Sorbonne University) is acknowledged for solving the structure of complex **5**. This work benefited from the support of the French National Research Agency (ANR) for the projects JCJC SMARTEES (15-CE07-0006- 01) and MULTIFUN (ANR-21-CE07-0013).

Notes and references

1. G. T. Morgan and F. H. Burstall, *J. Chem. Soc.*, 1932, 20-30.
2. a) M. Heller and Ulrich S. Schubert, *Eur. J. Org. Chem.*, 2003, **2003**, 947-961; b) R.-A. Fallahpour, *Synthesis*, 2003, 0155-0184.
3. a) A. Winter and U. S. Schubert, *Chemcatchem*, 2020, **12**, 2890-2941; b) S. Chakraborty and G. R. Newkome, *Chem. Soc. Rev.*, 2018, **47**, 3991-4016; c) S. M. Elahi, M. Raizada, P. K. Sahu and S. Konar, *Chem. Eur. J.*, 2021, **27**, 5858-5870; d) J. J. Shi and M. Wang, *Chem. Asian J.*, 2021, **16**, 4037-4048; e) J. E. M. Lewis and J. D. Crowley, *Chempluschem*, 2020, **85**, 815-827; f) C. Y. Wei, Y. He, X. D. Shi and Z. G. Song, *Coord. Chem. Rev.*, 2019, **385**, 1-19; g) X. J. Yu, C. X. Guo, S. Lu, Z. Chen, H. Wang and X. P. Li, *Macromol. Rapid Commun.*, 2022, **43**; h) V. Guerchais and J.-L. Fillaut, *Coord. Chem. Rev.*, 2011, **255**, 2448-2457.
4. a) Z. Gao, Y. F. Han, Z. C. Gao and F. Wang, *Acc. Chem. Res.*, 2018, **51**, 2719-2729; b) K. M. C. Wong and V. W. W. Yam, *Acc. Chem. Res.*, 2011, **44**, 424-434; c) V. W. W. Yam and Y. H. Cheng, *Bull. Chem. Soc. Jpn.*, 2022, **95**, 846-854; d) J. A. G. Williams, *Chem. Soc. Rev.*, 2009, **38**, 1783-1801; e) S. D. Cummings, *Coord. Chem. Rev.*, 2009, **253**, 449-478; f) E. V. Puttock, M. T. Walden and J. A. G. Williams, *Coord. Chem. Rev.*, 2018, **367**, 127-162; g) K. M. C. Wong and V. W. W. Yam, *Coord. Chem. Rev.*, 2007, **251**, 2477-2488; h) G. Romo-Islas, S. Burguera, A. Frontera and L. Rodríguez, *Inorg. Chem.*, 2024, **63**, 2821-2832; i) P.-H. Lanoë, J.-L. Fillaut, L. Toupet, J. A. G. Williams, H. L. Bozec and V. Guerchais, *Chem. Commun.*, 2008, 4333-4335; j) B. Hasenknopf, J. Hall, J.-M. Lehn, V. Balzani, A. Credi and S. Campagna, *New J. Chem.*, 1996, **20**, 725-730; k) B. Hasenknopf and J.-M. Lehn, *Helv. Chim. Acta*, 1996, **79**, 1643-1650.
5. A. Haque, L. Xu, R. A. Al-Balushi, M. K. Al-Suti, R. Ilmi, Z. Guo, M. S. Khan, W.-Y. Wong and P. R. Raithby, *Chem. Soc. Rev.*, 2019, **48**, 5547-5563.
6. a) M. Ueda, S. Horiuchi, E. Sakuda, Y. Nakao, Y. Arikawa and K. Umakoshi, *Chem. Commun.*, 2017, **53**, 6405-6408; b) J. Forniés, S. Fuertes, C. Larraz, A. Martín, V. Sicilia and A. C. Tsipis, *Organometallics*, 2012, **31**, 2729-2740.
7. a) J. Moussa, L. M. Chamoreau, M. P. Gullo, A. Degli Esposti, A. Barbieri and H. Amouri, *Dalton Trans.*, 2016, **45**, 2906-2913; b) M. Baya, Ú. Belío, J. Forniés, A. Martín, M. Perálvarez and V. Sicilia, *Inorg. Chim. Acta*, 2015, **424**, 136-149; c) S. Horiuchi, S. Moon, A. Ito, J. Tessarolo, E. Sakuda, Y. Arikawa, G. H. Clever and K. Umakoshi, *Angew. Chem. Int. Ed.*, 2021, **60**, 10654-10660.
8. a) B. Doistau, J.-L. Cantin, L.-M. Chamoreau, V. Marvaud, B. Hasenknopf and G. Vives, *Chem. Commun.*, 2015, **51**, 12916-12919; b) B. Doistau, A. Tron, S. A. Denisov, G. Jonusauskas, N. D. McClenaghan, G. Gontard, V. Marvaud, B. Hasenknopf and G. Vives, *Chem. Eur. J.*, 2014, **20**, 15799-15807; c) L. Benda, B. Doistau, C. Rossi-Gendron, L.-M. Chamoreau, B. Hasenknopf and G. Vives, *Commun. Chem.*, 2019, **2**, 144; d) B. Doistau, L. Benda, J.-L. Cantin, O. Cador, F. Pointillart, W. Wernsdorfer, L.-M. Chamoreau, V. Marvaud, B. Hasenknopf and G. Vives, *Dalton Trans.*, 2020, **49**, 8872-8882; e) B. Doistau, C. Rossi-Gendron, A. Tron, N. D. McClenaghan, L.-M. Chamoreau, B. Hasenknopf and G. Vives, *Dalton Trans.*, 2015, **44**, 8543-8551; f) B. Doistau, L. Benda, J.-L. Cantin, L.-M. Chamoreau, E. Ruiz, V. Marvaud, B. Hasenknopf and G. Vives, *J. Am. Chem. Soc.*, 2017, **139**, 9213-9220; g) P. Msellem, M. Dekthiarenko, N. Hadj Seyd and G. Vives, *Beilstein J. Org. Chem.*, 2024, **20**, 504-539.
9. a) E. Rajalakshmanan and V. Alexander, *Inorg. Chem.*, 2007, **46**, 6252-6260; b) J. P. Collin, S. Guillerez, J. P. Sauvage, F. Barigelletti, L. De Cola, L. Flamigni and V. Balzani, *Inorg. Chem.*, 1991, **30**, 4230-4238.
10. E. C. Constable, N. Hostettler, C. E. Housecroft, P. Kopecky, M. Neuburger and J. A. Zampese, *Dalton Trans.*, 2012, **41**, 2890-2897.
11. D. Rocco, C. E. Housecroft and E. C. Constable, *Molecules*, 2019, **24**, 1799.
12. a) Y. Chen, W. Lu and C.-M. Che, *Organometallics*, 2013, **32**, 350-353; b) W. A. Tarran, G. R. Freeman, L. Murphy, A. M. Benham, R. Kataky and J. A. G. Williams, *Inorg. Chem.*, 2014, **53**, 5738-5749; c) Y. Chen, K. Li, W. Lu, S. S.-Y. Chui, C.-W. Ma and C.-M. Che, *Angew. Chem. Int. Ed.*, 2009, **48**, 9909-9913; d) S. J. Farley, D. L. Rochester, A. L. Thompson, J. A. K. Howard and J. A. G. Williams, *Inorg. Chem.*, 2005, **44**, 9690-9703; e) Z. Wang, E. Turner, V. Mahoney, S. Madakuni, T. Groy and J. Li, *Inorg. Chem.*, 2010, **49**, 11276-11286; f) P. Pander, A. Sil, R. J. Salthouse, C. W. Harris, M. T. Walden, D. S. Yufit, J. A. G. Williams and F. B. Dias, *J. Mater. Chem. C*, 2022, **10**, 15084-15095.
13. a) K. Kotturi and E. Masson, *Chem. Eur. J.*, 2018, **24**, 8670-8678; b) H. Barbero and E. Masson, *Chem. Sci.*, 2021, **12**, 9962-9968; c) D. Prashar, Y. Shi, D. Bandyopadhyay, J. C. Dabrowiak and Y.-Y. Luk, *Bioorg. Med. Chem. Lett.*, 2011, **21**, 7421-7425.

14. a) X.-P. Zhang, V. Y. Chang, J. Liu, X.-L. Yang, W. Huang, Y. Li, C.-H. Li, G. Muller and X.-Z. You, *Inorg. Chem.*, 2015, **54**, 143-152; b) K. Li, Y. Chen, W. Lu, N. Zhu and C.-M. Che, *Chem. Eur. J.*, 2011, **17**, 4109-4112.
15. J. R. Berenguer, E. Lalinde and M. T. Moreno, *Coord. Chem. Rev.*, 2018, **366**, 69-90.
16. E. Rossi, A. Colombo, C. Dragonetti, D. Roberto, R. Ugo, A. Valore, L. Falciola, P. Brulatti, M. Cocchi and J. A. G. Williams, *J. Mater. Chem.*, 2012, **22**, 10650-10655.
17. J. Kuwabara, K. Yamaguchi, K. Yamawaki, T. Yasuda, Y. Nishimura and T. Kanbara, *Inorg. Chem.*, 2017, **56**, 8726-8729.
18. M. Hruzd, N. le Poul, M. Cordier, S. Kahlal, J.-Y. Saillard, S. Achelle, S. Gauthier and F. Robin-le Guen, *Dalton Trans.*, 2022, **51**, 5546-5560.
19. a) L. Stegemann, J. Sanning, C. G. Daniliuc and C. A. Strassert, *Z. Naturforsch., B: Chem. Sci.*, 2016, **71**, 1087-1093; b) K. Yamaguchi, K. Yamawaki, T. Kimura, J. Kuwabara, T. Yasuda, Y. Nishimura and T. Kanbara, *Dalton Trans.*, 2018, **47**, 4087-4092; c) R. J. Salthouse, A. Sil, L. F. Gildea, D. S. Yufit and J. A. G. Williams, *Inorg. Chem.*, 2023, **62**, 12356-12371.
20. J. Van Houten and R. J. Watts, *J. Am. Chem. Soc.* 1976, **98**, 4853-4858.
21. G. Sheldrick, *Acta Crystallogr., Sect. A*, 2015, **71**, 3-8.
22. G. Sheldrick, *Acta Crystallogr., Sect. C*, 2015, **71**, 3-8.